

Dynamic response of an offshore structure interacting with an ice floe failing in crushing

Hendrikse, Hayo; Nord, Torodd S.

DOI

[10.1016/j.marstruc.2019.01.012](https://doi.org/10.1016/j.marstruc.2019.01.012)

Publication date

2019

Document Version

Final published version

Published in

Marine Structures

Citation (APA)

Hendrikse, H., & Nord, T. S. (2019). Dynamic response of an offshore structure interacting with an ice floe failing in crushing. *Marine Structures*, 65, 271-290. <https://doi.org/10.1016/j.marstruc.2019.01.012>

Important note

To cite this publication, please use the final published version (if applicable).
Please check the document version above.

Copyright

Other than for strictly personal use, it is not permitted to download, forward or distribute the text or part of it, without the consent of the author(s) and/or copyright holder(s), unless the work is under an open content license such as Creative Commons.

Takedown policy

Please contact us and provide details if you believe this document breaches copyrights.
We will remove access to the work immediately and investigate your claim.

Green Open Access added to TU Delft Institutional Repository

'You share, we take care!' - Taverne project

<https://www.openaccess.nl/en/you-share-we-take-care>

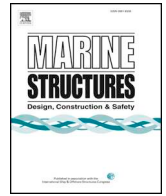
Otherwise as indicated in the copyright section: the publisher is the copyright holder of this work and the author uses the Dutch legislation to make this work public.



Contents lists available at ScienceDirect

Marine Structures

journal homepage: www.elsevier.com/locate/marstruc



Dynamic response of an offshore structure interacting with an ice floe failing in crushing



Hayo Hendrikse^{a,b,*}, Torodd S. Nord^b

^a Department of Hydraulic Engineering, Delft University of Technology, Stevinweg 1, 2628 CN, Delft, the Netherlands

^b Sustainable Arctic Marine and Coastal Technology, Norwegian University of Science and Technology, Høgskoleringen 7A, 7491, Trondheim, Norway

ARTICLE INFO

Keywords:

Intermittent crushing
Frequency lock-in
Continuous brittle crushing
Ice-induced vibrations
Ice engineering

ABSTRACT

Interaction of sea or lake ice with vertically sided offshore structures may result in severe structural vibrations commonly referred to as ice-induced vibrations. With the surge in offshore wind developments in sub-arctic regions this problem has received increased attention over the last decade, whereas traditionally the topic has been mainly associated with lighthouses and structures for hydrocarbon extraction. It is important for the safe design of these offshore structures to have the ability to predict the interaction between ice and structure in an expected scenario. A model for simulation of the interaction between a drifting ice floe and a vertically sided offshore structure is presented. The nonlinear speed dependent ductile and brittle deformation and local crushing of ice are considered phenomenologically. A one-dimensional sea ice dynamics model is applied to incorporate the effects of floe size, wind and current. The structure is modelled by incorporating its modal properties obtained from a general-purpose finite element software package. Alternatively, the model can be coupled to in-house design software for fully coupled simulations. Examples of application of the model to simulate dynamic ice-structure interaction are provided. Simulation results are validated with public data from forced vibration experiments, small-scale intermittent crushing and frequency lock-in, and full-scale interaction with the Norströmsgrund lighthouse. Effects of floe size and environmental driving forces on the development of ice-induced vibrations in full-scale are studied. It is shown that sustained frequency lock-in vibrations of the structure can only develop for very specific combinations of environmental driving forces and ice floe size. In all other cases, the ice floe slows down and comes to a stop, or accelerates to a drift speed which exceeds the range where frequency lock-in develops. This results in only a few cycles of vibration per interaction event, such as observed for the Norströmsgrund lighthouse in the Baltic Sea.

1. Introduction

Offshore structures in cold regions need to be designed to withstand the interaction with sea or lake ice. For vertically sided offshore structures, the interaction with an ice floe may result in severe structural vibrations, commonly referred to as ice-induced vibrations. Design standards provide simplified time traces of ice loads, which lead to such conservative structural responses that design for dynamic ice-structure interaction becomes challenging [1,2]. The main challenge remains to determine if a certain mode of ice-induced vibration can develop for a particular structure in particular ice conditions (i.e. intermittent crushing or frequency lock-in). Simulation models based on experimental and full-scale data provide an alternative to consider the dynamic interaction in a

* Corresponding author. Department of Hydraulic Engineering, Delft University of Technology, Stevinweg 1, 2628 CN, Delft, the Netherlands.
E-mail address: h.hendrikse@tudelft.nl (H. Hendrikse).

coupled manner, removing the need to determine the mode of interaction a priori. Model development has been ongoing since the first observations of ice-induced vibrations in the late sixties, and has been based mainly on two assumptions on the underlying physical mechanism.

The first approach applied is to assume a predefined (constant) global failure depth or crushing/spalling length of the ice [3,4]. Models including this assumption contain a periodicity in the ice load pattern which could explain the observations of frequency lock-in and intermittent crushing. Application of models based on this assumption shows that it is difficult to obtain good correspondence with measurements [5–7]. The extended approach developed by Sodhi includes, besides global loading and failure, extrusion of ice and the possibility for separation between ice and structure [8]. In that model, the crushing length is not predefined, but instead dependent on the interaction between ice and structure. As an alternative to the predefined global crushing length approaches, the effective negative damping approach is nowadays being more often applied, sometimes in combination with the predefined global crushing length [9–13]. This effective negative damping originates from the decreasing trend observed in the dependence of uniaxial compressive strength of ice on the rate by which the ice is loaded. The most detailed and most used model in the design of structures which is based on this approach is the PSSII model [10]. The PSSII model assumes local failure which allows for better reproduction of brittle crushing. The effective negative damping type of modelling requires a still debated assumption to be made with respect to the ice strength to match measurements of ice-induced vibrations. The strength of ice, and as a consequence the global load in the models, has to be assumed to reduce by approximately a factor two when the ice drift speed increases above 0.1 m s^{-1} [10].

Eight years were spent on developing a model for simulation of dynamic ice-structure interaction [14–16]. The aim of this development was to obtain a model which captures the local failure and deformation behavior of the ice at the ice-structure interface and does not assume a predefined global failure length or the debated stress-strain-rate dependence. The global and local failure and deformation of ice during indentation have been studied by experiments [16–18] and by re-analysis of existing full-scale data [19,20]. The work has been executed as part of the Norwegian Centre for Research Based Innovation ‘SAMCoT’ which has operated from 2011 and will end in 2019 [21].

In this paper we present our final simulation model as developed in the SAMCoT project. We summarize the experimental background referring to relevant material in existing publications and present the latest expansion of the model made to include driving forces acting on the ice floe in a simplified manner, allowing to apply the model to full-scale scenarios. New examples are presented to demonstrate and further validate the application of the model to simulate model-scale interaction during which intermittent crushing develops. The use of the model for full-scale simulations is demonstrated with an example of interaction observed at the Norströmsgrund lighthouse. A MATLAB implementation of the ice crushing part of the developed model is made publicly available as part of this publication, with the aim to facilitate its further development and use in the design of offshore structures [22].

2. Experimental background

A summary of experimental and full-scale background information is given. This experimental background covers the observations on dynamic ice-structure interaction which lie at the basis of the developed simulation model. The results from forced vibration experiments described in Ref. [18] complete the experimental basis, but are not repeated here.

First, general experimental and full-scale observations of ice action against relatively rigid structures are shown. We define rigid structures as structures being stiff and heavy, such that no interaction develops. The observations on local ice deformation and failure from ice action against rigid structures form the basis for the developed ice model. Second, observations on the interaction between ice and compliant structures resulting in intermittent crushing and frequency lock-in are presented.

It is emphasized that the focus here is mainly on the global observations since in our modelling the local interaction between ice and structure is considered in an approximate manner only. Research on local interaction between ice and structure is developing rapidly and promising for future model development. This research has, however, not yet matured enough in the past decade to make it applicable in simulation models and, as we believe the examples in Section 5 demonstrate, the level of detail it brings is not absolutely necessary to accurately simulate the global interaction between ice and structures.

2.1. Observations of ice action on rigid structures

A floe of ice acting on a vertically sided structure may fail in several ways depending on the indentation speed, aspect ratio, and ice properties [23,24]. At low speed, ice experiences significant creep. For high ratios between structure width and ice thickness, bending or buckling of the ice generally leads to relatively low loads. Ice-induced vibrations develop when the ice fails by crushing at speeds of loading exceeding those for which global creep is observed. We consider the case where the ice fails either by global creep or crushing.

Creep is relevant for dynamic ice-structure interaction as this deformation and failure mode occurs when the relative speed between the ice and structure becomes and remains small over a nontrivial amount of time. Creep is characterized by full contact between the ice and structure and a relatively uniform pressure at the ice-structure interface. Creep failure is characterized by large plastic deformation of the ice in front of the structure and material flowing slowly from the interface to form solidified ice in front and at the sides of the structure. This type of failure is sometimes referred to as ‘ductile failure’ in the context of ice-induced vibrations. Creep of ice is treated in detail in Refs. [25,26].

Crushing defines the ice deformation and failure at high indentation speeds and is characterized by local contacts and quasi-random ice load signals [27,28]. We use the term crushing to define the pulverization of ice directly in contact with the structure.

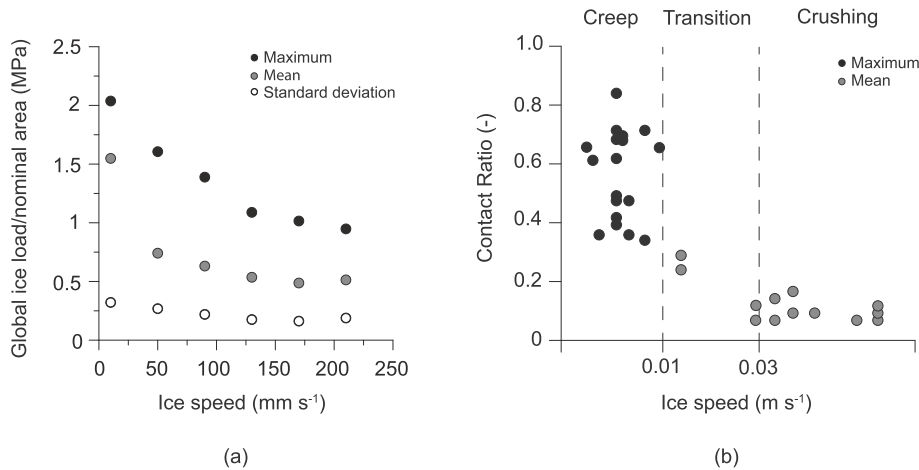


Fig. 1. (a) Statistical measures of the global load in crushing against a rigid structure at ice speeds exceeding those resulting in global creep of the ice. Data is replotted from Ref. [34]. (b) Dependence of contact ratio on indentation speed. Data is replotted from experiments by Ref. [36].

Formation of spalls and flakes as a result of cleavage cracks propagating to the free surface, and formation of radial cracks are not considered. Their effect on the variation of the global load can be significant, but these failure mechanisms are mainly disturbing the interaction process leading to ice-induced vibrations which are related to the smaller-scale processes at the contact. Spalls generally occur for aspect ratios, the ratio between structure width and ice thickness, above one, which is the range of interest for ice-induced vibrations of offshore structures. Also, spalls cause a wedge-shaped front of the ice when looking from the side. Radial crack formation does not necessarily have a measurable effect on the load on the structure [29]. Deformation of ice during crushing and prior to failure is mainly elastic at high indentation speeds. At indentation speeds close to the transition from creep to crushing, visco-elastic and visco-plastic deformation form a more pronounced part of the total deformation, even though the ice still crushes locally. A high degree of recrystallization of the ice directly in contact with the structure is often observed [30].

Typical time traces of the global ice load on a rigid structure in creep and crushing are presented, for example, in Ref. [31]. During creep, the global ice load increases gradually over time towards a peak value, after which the load reduces to a steady-state value [32]. In crushing, the time traces are generally quasi-random around a mean value, owing to the uncorrelated local failures in the contact zone between ice and structure. It is noted that the global ice load on a structure in crushing does not show a stationary global saw-tooth pattern as often observed in small-scale or wall-indentation tests where spalling is the dominant mode of failure [33].

Besides the time dependencies, the statistical measures of the global ice load are of importance for ice-structure interaction, especially the dependence on indentation speed of the maximum, mean, and standard deviation of the global ice load. Typical dependencies in the range where the ice fails in crushing are shown in Fig. 1a as reproduced from data from experiments with rigid indenters [34]. The global maximum load on a structure is largest at or around the transition speed, which marks the transition from creep to crushing, and this load can be up to four times the mean load during crushing at high speed [35]. The mean global ice load shows a reducing trend with indentation speed that eventually levels off, whereas the standard deviation remains more or less constant irrespective of ice drift or indentation speed [34].

The decrease in mean and maximum global load with increasing ice drift speed in the crushing range is of importance with respect to ice-induced vibrations. This dependence reflects the mechanism providing the energy from ice to structure required for the sustained and large-amplitude vibrations during frequency lock-in and intermittent crushing. The global load is generally considered as a summation of pressures in local contact areas where a distinction can be made between intact ice, which carries the majority of the load, and broken ice pieces or rubble, which do not generally carry a significant portion of the load. As such, the higher global ice load at the transition from creep to crushing can be a result of a larger contact area, higher pressures in individual contact zones, or both.

Results from field tests [36] show that the contact area between ice and structure changes significantly around the transition from creep to crushing. Results in terms of the contact ratio, defined as the area of contact between ice and structure over the total area, given by the ice thickness and structure width, are replotted in Fig. 1b. In creep, an almost full contact can be attained as indicated by the high values of the contact ratio, while during crushing the mean contact area is only roughly ten percent of the total area. A decreasing trend is observed starting from the transition between creep and crushing; however, the amount of data in this range is limited. Nevertheless, the contact area shows to change around the transition speed, indicating its role in the high loads observed at such speeds of indentation. Further experimental observations on the difference in contact area in the creep and crushing range can be found in Ref. [37] and from forced vibration experiments in Ref. [18]. With respect to pressures in the contact during indentation it is found that local peak pressures show to be generally higher in case of crushing at high indentation speeds, compared to creep at lower speeds [37].

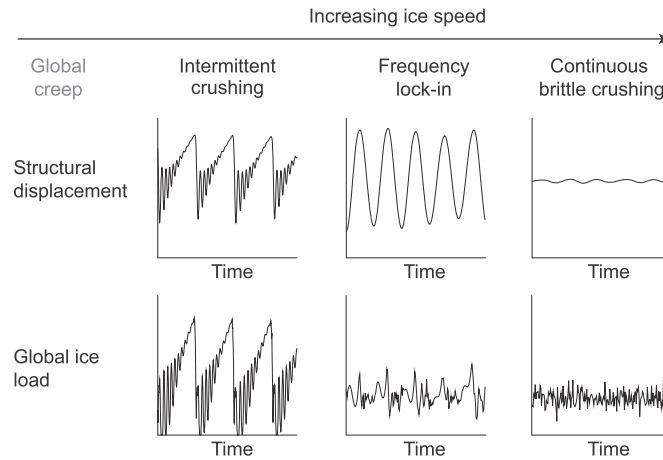


Fig. 2. Illustration of the structural displacement at the ice action point and the global ice loads in the three regimes of ice-induced vibrations.

2.2. Observations on dynamic ice-structure interaction

When a vertically sided compliant structure interacts with an ice floe, this can result in structural vibrations known as ice-induced vibrations. Three regimes of ice-induced vibrations are commonly distinguished: intermittent crushing, frequency lock-in, and continuous brittle crushing. An illustration of the time dependence of the global load and structural displacement in each of these regimes is provided in Fig. 2. Not all regimes develop for each type of compliant structure, but typically intermittent crushing is observed for the lowest indentation speeds, followed by frequency lock-in, and continuous brittle crushing at high indentation speeds. Intermittent crushing and frequency lock-in are of particular interest for the design of structures, as these types of interaction result in the largest global loads and amplitudes of structural oscillation. What follows is a summary of what we define as key observations for each of the interaction regimes. References to experimental and full-scale campaigns in which these key observations have been found are provided, but individual campaigns are not discussed.

Intermittent crushing develops when a relatively flexible structure with low stiffness at the location of ice action interacts with a slowly moving ice sheet [17,24,28,38–50]. Intermittent crushing is characterized by a sawtooth-like pattern in both the time traces of global ice load and structural displacement (Fig. 2). The sawtooth frequency is relatively constant for a particular structure in non-varying ice conditions, and increases with increasing ice drift speed, until frequency lock-in or continuous brittle crushing becomes the dominant mode of interaction [24]. The amplitude of structural displacement is mainly determined by the ratio between global ice load and structural stiffness. For this reason, the interaction is often referred to as ‘quasi-static’. Dynamic properties of the structure play a role in the transient structural response after an incident of global ice failure [17]. The large load drops are, in reality, a succession or cascade of brittle failures and not a single failure, but these load drops are nevertheless often referred to as simultaneous failure. The maximum global ice load during intermittent crushing is significantly larger than that observed during continuous brittle crushing. Reports from model-scale experiments indicate that the peak loads increase by a factor 1.7 up to 2.2 [40,43]. This increase is comparable to the increase in global ice load observed when ice failure against a rigid structure changes from crushing to creep, as described in the previous section. During the load build-up, the contact area between ice and structure shows to expand as pressures increase [14,17].

Frequency lock-in typically develops over a range of ice drift speeds for structures with low damping and low natural frequencies [32,35,40,43,45,48,51–57]. The vibrations are characterized by periodic oscillation of the structure at a frequency equal or slightly below one of the natural frequencies of the structure. The motion of the structure is close to harmonic with a small deviation at the time moment of major ice fracture (Fig. 2). At that moment, the ice temporarily prevents the structure from moving back towards its equilibrium position. The global ice load shows a quasi-random pattern, typical for crushing failure of ice, when the relative speed between ice and structure is high. A quick increase in global ice load is observed after a period of time during which the relative speed between ice and structure has been low. Often, a brief moment of reduction in ice load is observed as the structure temporarily moves faster than the ice, causing an unloading.

Frequency lock-in has mainly been observed to occur for structural vibration modes with natural frequencies in the range of 0 up to 10 Hz. To distinguish frequency lock-in from other types of periodic oscillation, the frequency lock-in relation can be used as guidance. During frequency lock-in, a more or less linear relation exists between the ice drift speed and the maximum velocity of the structure in the direction of ice motion. This relation has first been found by Toyama et al. [48] during model-scale experiments and confirmed by others [40,52,53,58]. The experimental results from these campaigns are replotted in Fig. 3. The relations between the maximum velocity of the structure in the direction of ice drift at the location of ice action and the ice drift speed is given by:

$$\dot{u}_{\max} = \beta v_{\text{ice}}, \quad (1)$$

where the value for β varies between 1.0 and 1.5 for the different experimental campaigns.

The effects of changes in structural stiffness and mass on the range of indentation speeds for which frequency lock-in develops

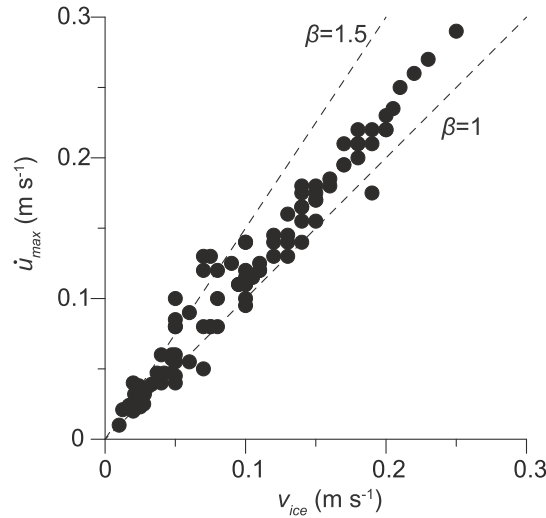


Fig. 3. Maximum velocity of the structure in the direction of ice drift plotted as a function of indentation speed during frequency lock-in. Results from several experimental campaigns are plotted [40,48,52,53,58].

have been studied in the experimental campaign by Huang et al. [52]. They found that the boundaries of the frequency lock-in regime shift to lower speeds with either increasing mass or natural frequency. Furthermore, the extent of the range shows to decrease. Note that Huang et al. draw a different conclusion from their results as they consider all effects to be attributed to the change in stiffness; however, as they simultaneously changed stiffness and mass, we find that the results have to be evaluated considering the simultaneous change of two properties.

Continuous brittle crushing develops for all structures at high ice drift speeds. The ice load fluctuates around a mean value in the case of stationary ice conditions. Structural oscillations are typical for a structure excited by a stochastic aperiodic load. The amplitude of oscillation of the structure and maximum global ice load are significantly smaller than those observed in the frequency lock-in and intermittent crushing regimes. The ice deformation and failure during continuous brittle crushing are in fact the same as for rigid structures at high ice drift speeds (i.e. local and concentrated on a line), indicating that the interaction between ice and structure is insignificant at these high speeds.

3. Ice model

A phenomenological model was developed to reproduce the global observations on ice deformation and failure described in Section 2.1 and [18]. The model has been described in Ref. [16], but the mathematical description of the model and definition of input parameters are provided here for completeness and clarity. The model is one-dimensional, simulating the ice load in the direction of ice drift. To capture the stochastic nature of the brittle crushing process, the ice is partitioned in N elements (Fig. 4b). The elements are independent and initially positioned with an offset to the structure obtained from a uniform distribution U , resulting in an effective roughness of the ice edge:

$$u_{i,1} = u_{i,2} = u_{i,3} = u_{s,0} - U(0, r_{\max} + v_{ice} t_f) \quad (2)$$

with r_{\max} the maximum offset of an element with respect to the structure, $u_{s,0}$ the initial position of the structure, and t_f the time between initial contact and failure for an individual ice element at an ice drift speed v_{ice} , assuming a rigid structure. $v_{ice} t_f$ is added to r_{\max} for the initial ice element positions only and to ensure that the initial distribution of elements is similar to the distribution

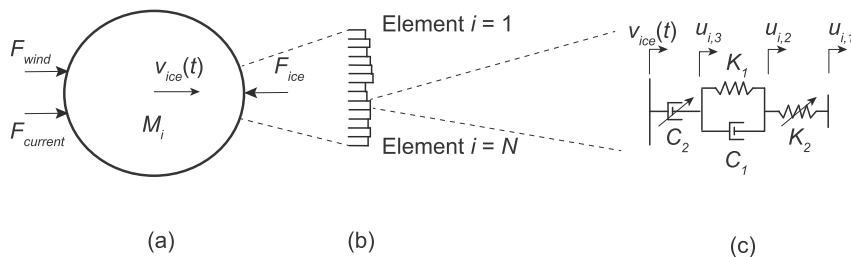


Fig. 4. (a) Ice drift model incorporating a single effective ice floe and wind and current driving forces. (b) The ice edge modelled as N independent elements with an individual offset to the structure to incorporate the roughness of the ice edge. (c) Each ice element modelled as a combination of springs and dashpots to capture elastic, delayed-elastic and viscous deformation.

occurring during interaction. The magnitude of t_f is obtained by solving Eq. (5) below using $N = 1$, $u_{i,1} = u_s = 0$, $u_{i,2}(t = t_f) = \delta_f$.

Each element moves towards the structure with the ice drift speed $v_{ice}(t)$, which can be either predefined or obtained based on the ice drift equation introduced in Section 3.2. Upon contact, the local deformation and failure behavior of the ice is modelled by a combination of springs and dashpots (Fig. 4c). The front non-linear spring with stiffness K_2 captures the local elastic deformation of the ice and failure in crushing upon reaching a predefined critical local deformation. The spring cannot transmit a load in tension, nor any load exceeding its critical load:

$$\begin{aligned} K_2 &= K_2 \quad \text{for} \quad 0 < u_{i,2} - u_{i,1} \leq \delta_f \\ K_2 &= 0 \quad \text{else} \end{aligned} \quad (3)$$

The middle linear spring-dashpot combination with damping coefficient C_1 and spring stiffness K_1 is included to reproduce the delayed-elastic deformation of the ice. The rear non-linear dashpot with coefficient C_2 is added to simulate the power-law creep deformation. Note that the dimension of C_2 is $[N^3 \text{ m}^{-1} \text{ s}]$ and that the load transferred by the dashpot is defined as:

$$F_{C2} = \sqrt[3]{C_2(v_{ice} - \dot{u}_{i,3})} \quad (4)$$

The equations of motion for an individual ice element are defined as:

$$\begin{aligned} u_{i,1} &= \begin{cases} u_{i,2} & u_{i,1} < u_s \\ u_s & u_{i,1} \geq u_s \end{cases} \\ \dot{u}_{i,2} &= \frac{K_2}{C_1}(u_{i,1} - u_{i,2}) + \frac{K_1}{C_1}(u_{i,3} - u_{i,2}) + v_{ice} - \frac{1}{C_2}(K_2(u_{i,2} - u_{i,1}))^3 \\ \dot{u}_{i,3} &= v_{ice} - \frac{1}{C_2}(K_2(u_{i,2} - u_{i,1}))^3 \end{aligned} \quad (5)$$

with $u_{i,1}$, $u_{i,2}$, and $u_{i,3}$, the three degrees of freedom of the ice element and u_s the displacement of the structure at the location where the ice load acts. This results in a speed dependent deformation and failure behavior of the individual ice elements as shown in Fig. 5. At high speeds, the behavior is elastic until the predefined critical local deformation δ_f is reached. At low speeds, the viscous-elastic behavior of the elements results in a significantly larger deformation of the elements prior to failure. Note that this results in critical deformation of the ice upon which failure occurs that is dependent on both ice speed and the interaction with the structure, despite the local crushing deformation δ_f being predefined.

Elements in contact with the structure deform, resulting in a global load on the structure given by:

$$F_{ice}(u_s, t) = \sum_{i=1}^N F_i = \sum_{i=1}^N K_2(u_{i,2} - u_{i,1})H(u_{i,1} - u_s), \quad (6)$$

With F_i the contribution to the global load of a single ice element and H the Heaviside step function indicating contact or no contact between an ice element and the structure. Upon failure of an element, it is removed from the model and replaced by a new element with an initial position offset from the structure:

$$u_{i,1} = u_{i,2} = u_{i,3} = u_{s,0} - U(0, r_{max}) \quad (7)$$

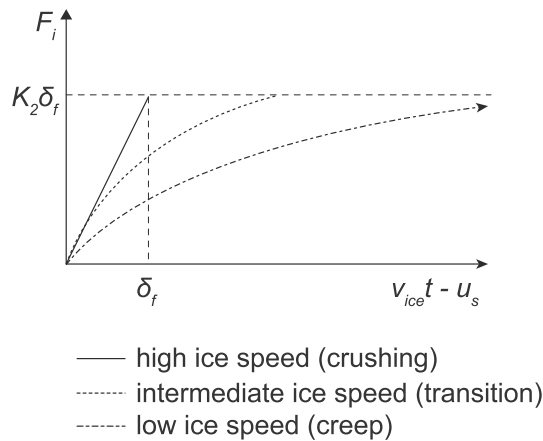


Fig. 5. Local ice load transferred by an ice element versus the total deformation of an ice element $v_{ice}t - u_{i,1}$, under the assumption of a constant ice speed and first contact at $t = 0$ against a rigid structure i.e. $u_{i,1} = u_s = 0$. At high ice speeds, the deformation grows approximately linearly until it equals the predefined local crushing deformation, upon which brittle failure is defined to occur and the element is removed and repositioned based on Eq. (7). At low ice speeds, brittle failure never occurs due to the large deformations in the rear dashpot element (C_2). At intermediate speeds, around the transition from ductile to brittle ice behavior in the model, local brittle failure develops after a total element deformation is reached which exceeds the predefined critical deformation δ_f .

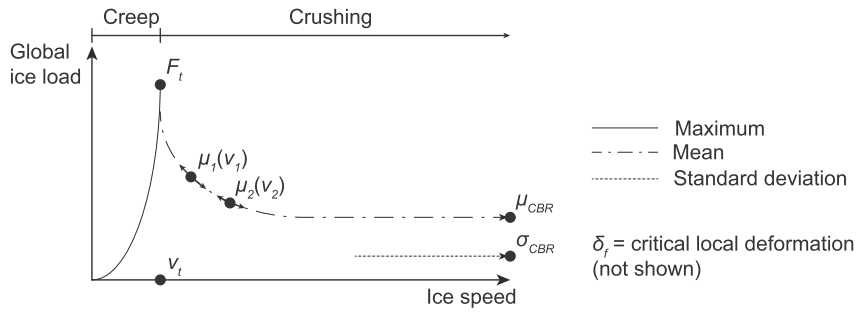


Fig. 6. Trends in global ice load on a rigid structure [34]. The seven parameters of the ice model are defined such that the model matches the six points on the curve and the critical local deformation (not shown). The seven data points used to define the seven model parameters are: Continuous brittle crushing mean load μ_{cbr} , critical local deformation δ_f , continuous brittle crushing standard deviation σ_{cbr} , ice speed where the transition between global creep and crushing occurs v_t , the maximum global load at this ice speed F_t , and two additional points defining the dependence of mean load on ice drift speed (μ_1, μ_2). Note that, this curve is considered to be uniquely defined for a given interaction scenario defined by the ice and its properties and the interaction area, defined by the projected structural width.

3.1. Definition of model input parameters

The ice model described in the previous section requires seven ($K_1, K_2, C_1, C_2, N, r_{max}, \delta_f$) input parameters to be defined which, due to the phenomenological nature of the model, have to be obtained based on measurements. These measurements are used to define the ice load on a rigid (immobile) structure, which then allows for simulation of any flexible structure in ice conditions similar to those from which the ice load measurements were obtained. The approach for defining the ice load on a rigid structure is described here. An example of the determination of the parameters for model-scale ice in the HSVA ice basin is given in Ref. [16].

For a rigid structure, the trends in global ice load, as shown in Fig. 1a, can be uniquely defined by six points, as indicated in Fig. 6. These six points implicitly contain the effects of ice thickness, ice strength, temperature, grain size, etc. The seventh data point required to define the seven model parameters is the aforementioned local critical deformation for ice crushing at high ice speed. This parameter is defined separately as it relates more to local crushing of ice at the ice-structure interface. A discussion on this parameter is included in Ref. [16]. The model parameters are defined such that the model exactly reproduces the statistical measures indicated by the six points in Fig. 6, and the trends indicated by the lines.

Once the magnitudes of the six points indicated in Fig. 6, as well as the critical local deformation, have been obtained from measurements, five of the model parameters can be defined explicitly based on the following set of equations:

$$\begin{aligned}
 \delta_f &= \delta_f \\
 r_{max} &= \delta_f \left(\frac{F_t}{\mu_{cbr}} - 2 \right) \\
 N &= \frac{\left(\frac{2F_t}{3\mu_{cbr}} - 1 \right)}{\left(\frac{\sigma_{cbr}}{\mu_{cbr}} \right)^2} \\
 K_2 &= \frac{F_t}{\delta_f N} \\
 C_2 &= \frac{F_t^3}{N^3 v_{ice}}
 \end{aligned} \tag{8}$$

Eq. (8) shows a limitation of this approach, being that the maximum load F_t needs to exceed 1.5 times the mean load μ_{cbr} for the number of elements to be positive, and to exceed twice the mean load for a positive effective roughness of the ice edge, indicated by the value of r_{max} . Experimental observations indicate that this is often the case [16,40,43]. The final two parameters, K_1 and C_1 , can be found by solving for the expected value of the global ice load in Eq. (6) for ice action against a non-moving structure, setting u_s to zero in Eq. (5):

$$\begin{aligned}
 \mu_1(v_1) &= \frac{F_t \int_0^{t_f(v_1)} u_{i,2}(t) dt}{\delta_f \frac{0.5r_{max}}{v_1} + t_f(v_1)} \\
 \mu_2(v_2) &= \frac{F_t \int_0^{t_f(v_2)} u_{i,2}(t) dt}{\delta_f \frac{0.5r_{max}}{v_2} + t_f(v_2)}
 \end{aligned} \tag{9}$$

This set of equations presents an optimization problem which can be solved iteratively after the first five parameters have been defined based on Eq. (8).

The model parameters need to be adjusted, or scaled, for simulation of structures with different size, or ice with different properties from those used to define the six points in Fig. 6. A larger ice thickness, for example, results in a larger magnitude of the mean load levels, max load level, and the standard deviation. A wider structure results in larger ice load values, but additionally a

lower ratio between standard deviation and mean load in brittle crushing [34]. The curve is uniquely defined for a specific interaction scenario, but the problem of how to scale it for changes in ice properties remains unsolved, and therefore this has to be done on a case-by-case basis using knowledge of ice mechanics and available data sources.

3.2. Extension of the model to include ice drift

In simulations where the ice drift speed is assumed constant, the described model can be directly applied. In full-scale scenarios, the ice drift velocity is often not constant as ice floes slow down or accelerate towards an offshore structure. In order to make the model better applicable to simulate full-scale interaction, we expanded the model to consider the effects of floe size, wind, and sea current in a simplified manner based on the work by Leppäranta [59]. An additional degree of freedom x_{ice} is introduced to simulate the drift of a single equivalent cylindrical ice floe, representing the pack ice, with diameter d_i (Fig. 4a). The equation of motion for the floe is given by:

$$\rho_i h_i \ddot{x}_{ice} = \rho_w C_{d,w} \text{sgn}(v_w - \dot{x}_{ice})(v_w - \dot{x}_{ice})^2 + \rho_a C_{d,a} v_a^2 - \frac{F_{ice}(u_s, t)}{\frac{\pi}{4} d_i^2}, \quad (10)$$

Where ρ_i is the density of the ice, h_i the ice thickness, ρ_w the density of the water, ρ_a the density of air, v_w the current speed in direction of the structure, v_a the wind speed in the direction of the structure, $C_{d,w}$ the water drag coefficient, and $C_{d,a}$ the air drag coefficient. To include this drift model, v_{ice} in Eq. (2) is replaced by $\dot{x}_{ice,0}$ and in Eq. (5) by $\dot{x}_{ice}(t)$.

4. Structural model and solution method

The ice model described in the previous section can be straightforwardly coupled to in-house software for structural design to run fully-coupled simulations. This is the preferred approach when other non-linear effects are to be included in the simulation such as those originating from aerodynamic interaction or non-linear soil-structure interaction. When such non-linear effects are not part of the simulation, the structure can be considered in the modal domain resulting in the following system of equations for the structure:

$$\ddot{\eta}_i + 2\xi_i \omega_i \dot{\eta}_i + \omega_i^2 \eta_i = f_i \left(t, \sum_{i=1}^n \phi_i^{ice} \eta_i \right), \quad i = 1, 2, \dots, n \quad (11)$$

where η_i is the modal amplitude of mode i , and ω_i the corresponding modal frequency. It is assumed here that the modal matrix Φ is constructed with the mass-orthonormalized vibration modes such that the modal mass matrix reduces to the identity matrix. Furthermore, an artificial diagonal modal damping matrix is introduced, with modal damping coefficients ξ_i . The modal forces f_i are given here by the contribution of the global ice load to each mode which corresponds to the modal amplitude at the ice action point ϕ_i^{ice} multiplied by the global ice force (Eq. (6)):

$$f_i \left(t, \sum_{i=1}^n \phi_i^{ice} \eta_i \right) = \phi_i^{ice} F_{ice} \left(\sum_{i=1}^n \phi_i^{ice} \eta_i, t \right), \quad i = 1, 2, \dots, n \quad (12)$$

Note that the global ice force couples all modes through the displacement of the structure at the ice action point. Additional forces on the structure can be straightforwardly included in the modal forces in Eq. (11).

A MATLAB implementation of the model, including a single-degree-of-freedom structural representation in the modal domain, is available from Mendeley data [22]. We solve the system of equations given by Eqs. (2)–(7) and Eq. (11) and (12) using the MATLAB ode23 solver and event detection to handle failure of the ice. An adaptive time-stepping scheme is used to optimize the time step, which can become very small at high drift speeds as all individual crushing events need to be processed. Note that, for computational reasons, the Heaviside function in Eq. (6) is approximated by a hyperbolic tangent. The shared model code does not include the pre-processing tools used to generate the ice input parameters for different scenarios, nor does it include the ice drift module. Examples of input parameter sets for the model are provided in Table 1 in Section 5.

5. Examples of application of the model

Examples are presented to demonstrate and validate the application of the model to simulate dynamic ice-structure interaction. For the small-scale examples, we based the model input parameters (Table 1) on those determined for the HSVA model ice [16]. The reason for this is twofold. First, we do not have access to the test data required to perform the procedure of obtaining the parameters for different ice types. Second, the results obtained this way illustrate that the model is not very sensitive to the choice of parameters and can give good results for a wide range of application, despite the input parameters not being optimized for the ice type considered. For the full-scale scenario in Section 5.4, a separate parameter set has been defined based on full-scale data from the STRICE campaign, see for example [30]. Effects of ice drift on the interaction are treated in Section 6.

Table 1

Model parameters used for simulation of the examples in Sections 5.1 to 5.4.

#	Interaction mode	Structure Configuration	K_1 (N m ⁻¹)	K_2 (N m ⁻¹)	N (-)	C_1 (N m ⁻¹ s)	C_2 (N ³ m ⁻¹ s)	δ_f (m)	r_{\max} (m)
1	Forced harmonic	Rigid	$1.64 \cdot 10^4$	$2.38 \cdot 10^5$	43	$1.24 \cdot 10^5$	$2.14 \cdot 10^{11}$	0.002	0.0029
2	Intermittent crushing	MDOF	$2.43 \cdot 10^4$	$3.52 \cdot 10^5$	43	$1.84 \cdot 10^5$	$6.99 \cdot 10^{11}$	0.002	0.0029
3	Frequency lock-in	SDOF	$3.96 \cdot 10^3$	$3.75 \cdot 10^4$	156	$1.25 \cdot 10^4$	$4.22 \cdot 10^8$	0.002	0.0029
4	Frequency lock-in	SDOF	$2.01 \cdot 10^4$	$1.91 \cdot 10^5$	15	$6.38 \cdot 10^4$	$5.55 \cdot 10^{10}$	0.002	0.0029
5	Continuous brittle crushing/Frequency lock-in	MDOF	$1.38 \cdot 10^7$	$5.28 \cdot 10^7$	58	$4.96 \cdot 10^7$	$4.71 \cdot 10^{18}$	0.004	0.006

#	ω_i (rad s ⁻¹)	ξ_i (-)	ϕ_1^{ice} (-)
1			
2	MDOF structure [14]		
3	68.5	0.025	0.0436
4	7.98	0.0023	0.0101
5	MDOF structure [16]		

5.1. Simulation of forced-vibration experiments

The forced vibration experiments described in Ref. [18] show how the global load on the structure changes when the relative speed between ice and structure reduces to low values, resulting in an increase in contact area and global load. We simulated one forced vibration test at 40 mm s^{-1} indentation speed with a fixed structural oscillation amplitude of 11 mm and frequency of oscillation of 0.57 Hz. The structure was cylindrical with a width of 220 mm and was subjected to 60 mm thick HSVA model ice with a compressive strength of 270 kPa, a salinity of 3.3 ppt, an average flexural strength of 150 kPa, and temperature of -2° Celsius. The resulting average brittle crushing load in the experiment was 7 kN. A picture of the structural setup is included in Fig. 7.

Input parameters for the ice model are defined in Table 1 (#1). The model ice used in the DIIV campaign was significantly more brittle compared to the IVOS campaign [60,61]. We did not test a rigid structure at the time, which would have allowed us to define input parameters for the more brittle case and study how brittleness factors into the model parameters. Nevertheless, an increased brittleness is accounted for by reducing the transition speed from creep to crushing in the model (Fig. 6) from 1 mm s^{-1} as obtained for the IVOS campaign in Ref. [16] to 0.5 mm s^{-1} and shifting the location of points v_1 and v_2 accordingly (Fig. 6).

Fig. 8 shows the simulated and experimentally obtained global ice load. The model captures the change in behavior when moving from high relative speed to lower relative speeds. The brittle crushing loads obtained from the model are in good agreement with the measured loads, whereas the peak loads are underpredicted. One observable difference between experimental load and simulated load (Fig. 8a and b) is that a load reduction occurs in the model during the time where brittle crushing is temporarily halted, which is observed to be not that significant in the tests. When the relative speed does not reach zero in the simulations, the load reduction disappears and peak loads increase to the levels observed in the experiments (Fig. 8c). The difference can either originate from the experiments, where we are not certain of the velocity control of the structural motion, from the modelling approach, where the chosen phenomenological ice elements start to unload before the actual relative speed becomes zero, or from the input parameters as

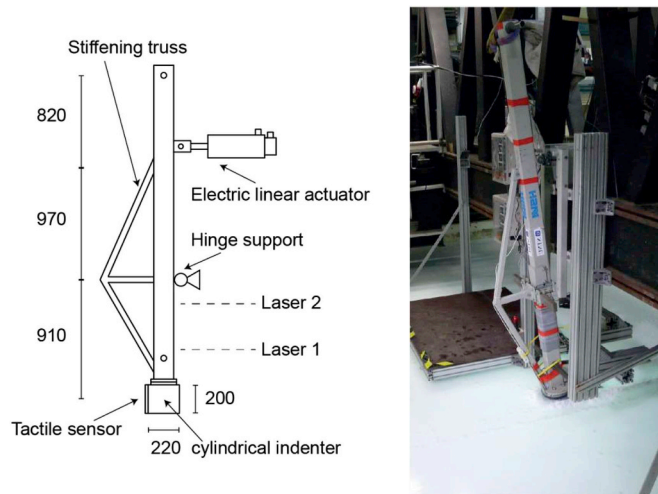


Fig. 7. Structural setup in the DIIV campaign [60]. The sketch shows the forced vibration setup [17]. For the free vibration tests as described in Section 5.2, the actuator was replaced by a spring support [18,60].

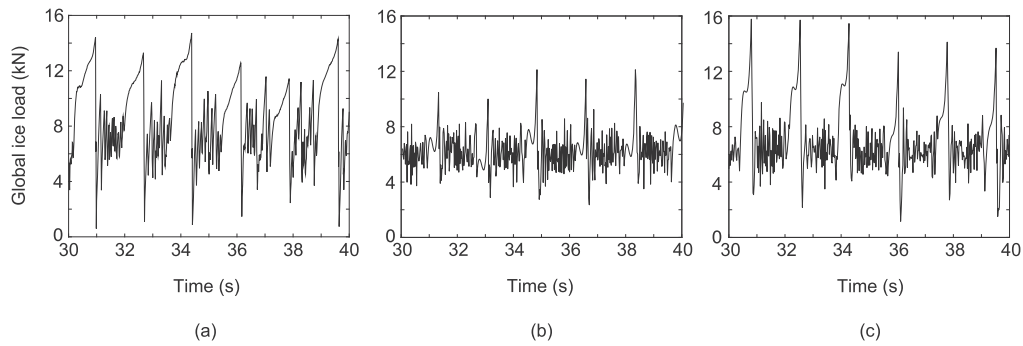


Fig. 8. A forced oscillation experiment at an indentation speed of 40 mm s^{-1} with an amplitude of 11 mm and frequency of oscillation of 0.57 Hz. (a) Experimentally obtained global load signal [18]. (b) Simulation results (c) Simulation results with reduced amplitude of oscillation to 10.2 mm.

the ice may have been more ductile than currently modelled.

5.2. Model-scale intermittent crushing

To validate that the model can reproduce interaction with a flexible structure leading to intermittent crushing, a case is simulated and compared with measurements from the Deciphering Ice Induced Vibrations (DIIV) campaign test 4300 [60]. The structure used for the free vibrations in the DIIV campaign (Fig. 7) was designed with the specific aim to have the two lowest modes both susceptible to frequency lock-in to confirm or reject the hypothesis that such type of structure would show frequency lock-in in the first mode at low indentation speeds, and then transition to the second mode with an increase in indentation speed. Unfortunately, we mainly observed intermittent crushing in the experiments.

To simulate the DIIV tests, we derived the structural matrices from the multi-degree-of-freedom structural model described in Ref. [17]. The structural model used in the free vibration experiments was the same as that for the forced vibration experiments shown in Fig. 7, except that the linear actuator was removed and replaced by a spring support. The HSVA model ice was 60 mm thick, was tested at -1.7° Celsius, and had 3.2 ppt salinity and a flexural strength of 150 kPa. The ice used in the free vibration experiments had a higher compressive strength of 400 kPa, compared to the 270 kPa for the forced vibration experiments described in Section 5.1, which is why there is a factor 400/270 difference in the magnitude of the model parameters associated with the ice strength in Table 1 (#1 and #2).

A comparison of the measured displacement response of the structure and the simulated one for an indentation speed of 0.05 m s^{-1} is shown in Fig. 9. Intermittent crushing develops with a non-constant amplitude of oscillation of the structure. The reason the saw-tooth pattern can develop up to such high speeds is that the first natural frequency of the model at 12.1 Hz is relatively high. What we could not explain at the time is why clear stationary frequency lock-in was not observed during the tests, whilst the velocity amplitude of oscillation was often in the range and even exceeded the values associated with frequency lock-in based on the equation introduced in Section 2.2.

We simulated the response of the structure for indentation speeds between 0.02 m s^{-1} up to 0.3 m s^{-1} which is the range tested in the experiment (Fig. 10). The results for the peak structural velocity amplitude (Fig. 10b) show that indeed peak amplitudes are high over the entire range of drift speeds, exceeding the magnitudes commonly associated with frequency lock-in. Studying in more detail the time dependence of the structural velocity for an indentation speed of 0.28 m s^{-1} (Fig. 10c), both the first and second mode

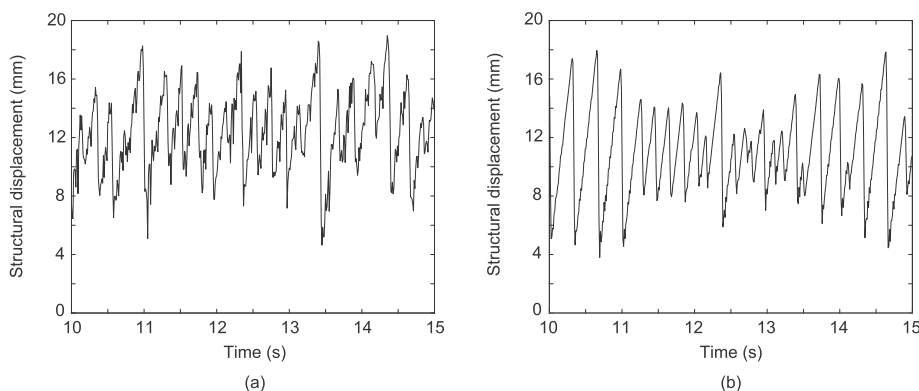


Fig. 9. Structural displacement at the ice action point during DIIV test 4300 at 0.05 m s^{-1} indentation speed. (a) Laser measurements from the experiments and (b) simulation results.

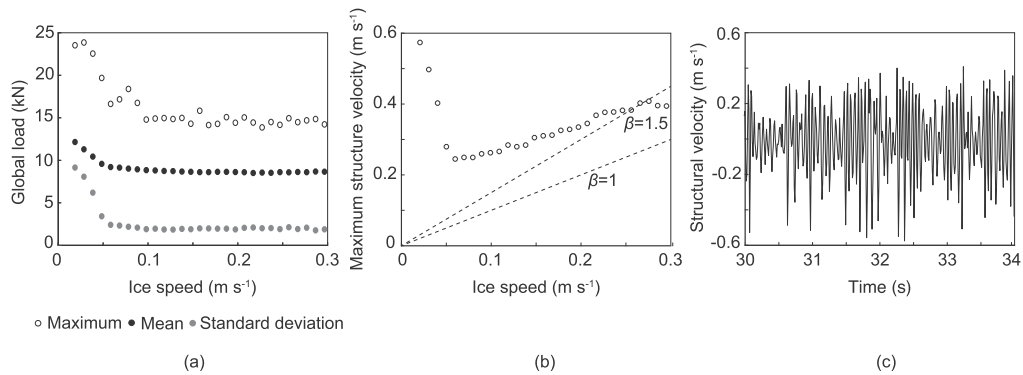


Fig. 10. (a) Simulated measures of global load, compare to Nord et al. [17, Fig. 7a]. (b) Simulated peak velocity amplitude of the structure. (c) Simulated structural displacement at the ice action point for an ice drift speed of 0.28 m s^{-1} .

appear to be active. Peak velocities mostly originate from oscillations in the second mode. These results indicate that the failure to obtain frequency lock-in in the DIIV experiments is likely to have originated from the structural design, with two closely spaced modes with approximately equal damping and oscillating mass at the ice action point. Both of the modes being easily excited by the ice removes the possibility for one of them to control the interaction, which is a requirement for sustained frequency lock-in.

5.3. Model-scale frequency lock-in

An example comparison of model simulations and experimental observations of frequency lock-in for a structure with a natural frequency of 5.4 Hz in HSVA model-ice can be found in [16, Fig. 17]. Here we present two additional model-scale examples to demonstrate the capabilities of the model (Table 1 (#3,#4)).

The first example is one used by Kärnä et al. [10, Fig. 11] in validation of the PSSII model. This example demonstrates frequency lock-in at a high natural frequency of 10.9 Hz. The tests were conducted in granular grained urea ice with a compressive strength in the range of 115 kPa up to 300 kPa [44]. Simulated time traces of the structural displacement, velocity, and global ice load (Fig. 11) show lock-in to develop as observed in the experiments. Correspondence is found in the amplitude of structural displacement and velocity. Minor differences exist between the simulated mean displacement and that measured in the original experiments and are believed to originate from a mismatch between true and reported structural stiffness and natural frequency during the experiment.

The second example is that of frequency lock-in at a low natural frequency in model-scale. Toyama et al. [48] tested a structure

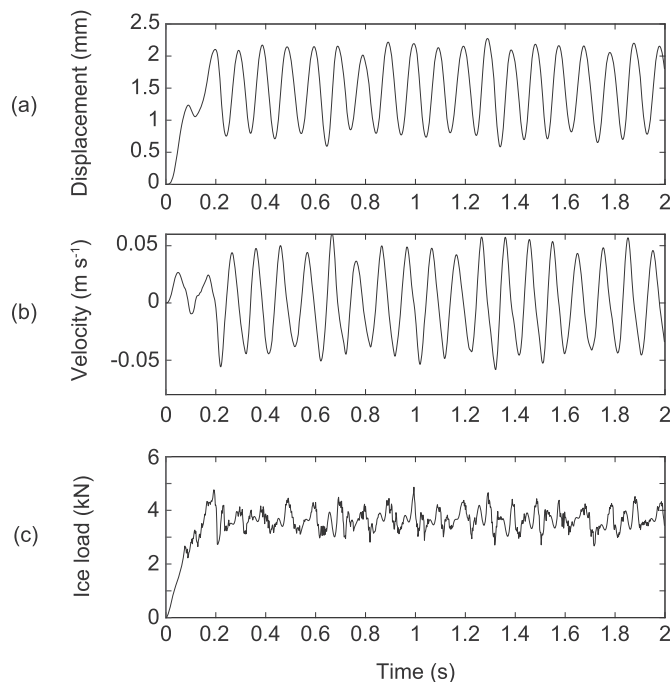


Fig. 11. Time traces of (a) structural displacement, (b) structural velocity, and (c) global ice load. For comparison to Kärnä et al. [10, Fig. 11].

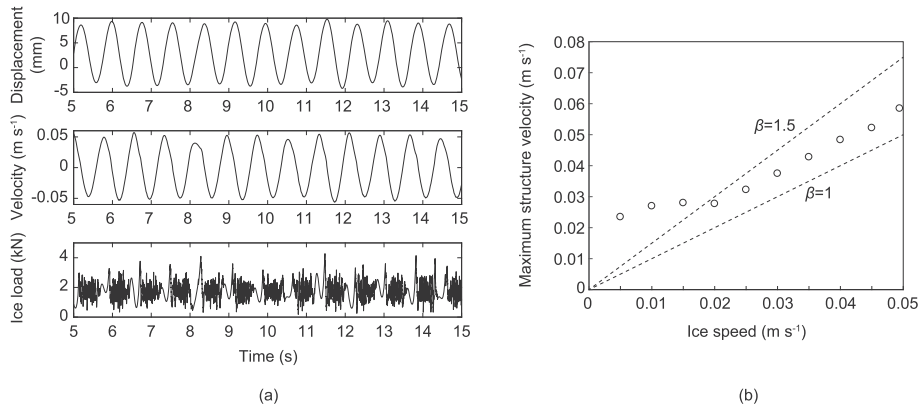


Fig. 12. Simulation results for the experiments performed by Ref. [45]. (a) Structural displacement, velocity, and global ice load for a simulation at 0.048 m s^{-1} ice drift speed and 0.039 m ice thickness. (b) Structural velocity amplitude plotted against ice drift speed. Frequency lock-in develops between 0.02 and 0.05 m s^{-1} for which the amplitudes follow the relationship given by Eq. (1).

with a first natural frequency of 1.27 Hz which, to our knowledge, is the lowest frequency in literature for which frequency lock-in has been observed in model-scale. Lock-in developed at speeds between 0.015 m s^{-1} and the maximum tested indentation speed of 0.048 m s^{-1} [45, Fig. 4]. Natural saline ice was used in the experiments. The simulation for an ice thickness of 0.039 m at an ice drift speed of 0.048 m s^{-1} (Fig. 12a) shows frequency lock-in to develop with an oscillation amplitude of 7 mm . We found a range of indentation speeds for which frequency lock-in develops comparable to that reported (Fig. 12b) The model predicts structural velocity amplitudes during frequency lock-in which are in accordance with the general relationship given by Eq. (1).

5.4. Full-scale interaction at the Norströmsgrund lighthouse

Here the results are presented from a simulation of an event of full-scale interaction at the Norströmsgrund lighthouse recorded during the STRICE campaign on April 5th, 2001, and described in Ref. [20] and in detail in Ref. [62]. The original measurements of the global ice load and structural accelerations at two heights along the lighthouse are shown in Fig. 13. Note that the load measurements have been corrected for panel coverage based on the method used in the ice-induced vibrations JIP [5]. During this event,

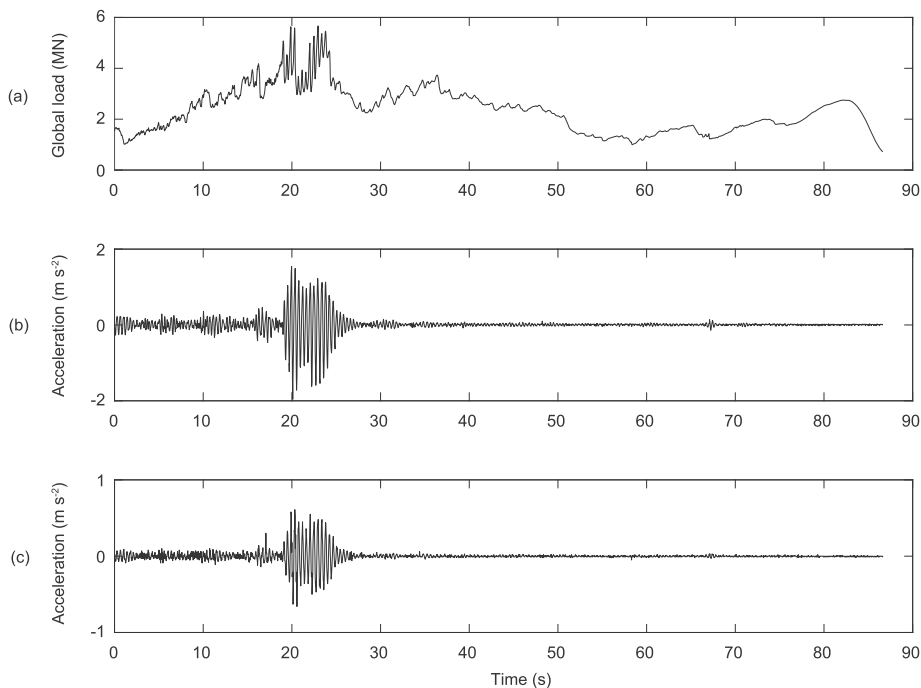


Fig. 13. Measurements of global load (corrected for panel coverage) (a) and structural acceleration (b,c) on April 5th, 2001 at the Norströmsgrund lighthouse [62]. Ten cycles of frequency lock-in develop 19 s in as the ice sheet slows down and global loads increase. Frequency lock-in disappears when the ice floe slows down to further deform in creep.

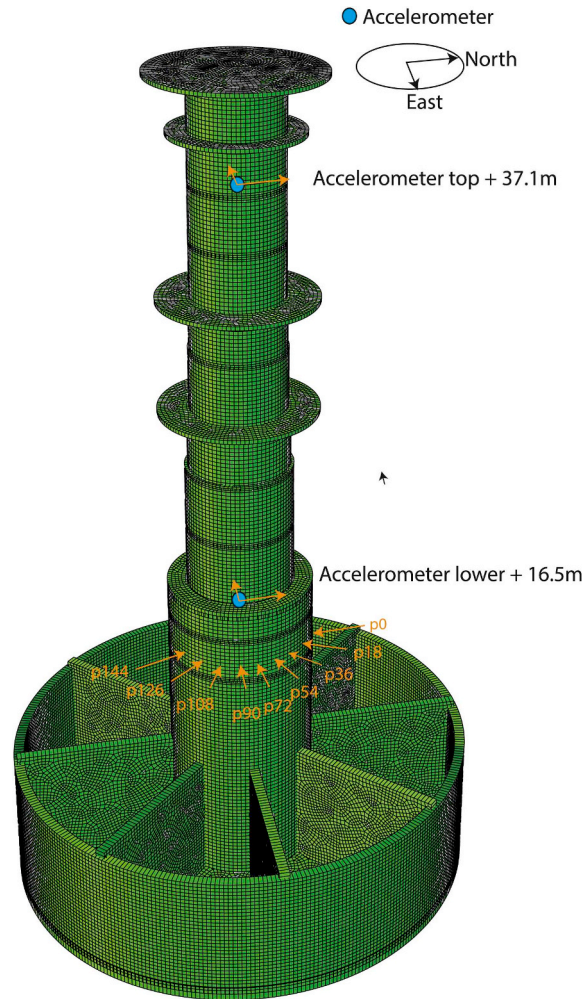


Fig. 14. Finite element model of the lighthouse used for the simulation. For details about the model see Ref. [16] and Table 3.

the ice floe was slowing down from 0.1 m s^{-1} to eventually come to a rest and deform in a creep manner. While slowing down, frequency lock-in suddenly developed and sustained for about ten cycles before the ice floe speed reduced to speeds at which the ice no longer failed in crushing. This type of observation is typical for the lighthouse where sustained vibration did not occur often and most events only lasted a few cycles [20].

To simulate this event, we used a finite element model of the lighthouse presented in Ref. [19]. An illustration of the model and its properties is given in Fig. 14. The first 12 bending modes were included in the simulation (Table 2.). Rayleigh damping with 2% of critical for modes 1 and 2, and 20% of critical for modes 23 and 24 was included. The ice load was applied on the structural node facing the North direction. On April 5, 2001 the ice floe was actually drifting in from the South-East; however, because of the axis symmetry of the finite element model, the results of the simulation are independent of the direction of application of the ice load. The application of the load in North-South direction allows us to obtain the resulting accelerations directly from the simulated accelerometers already available in the model. Ice was assumed to act over the entire width of the structure and a brittle crushing mean load of 3.5 MN was assumed based on the time of relatively steady crushing between 15 and 25 s in Fig. 13. Note that the load buildup seen in Fig. 13 suggests that the contact or ice thickness changed during the interaction; however, we did not consider this in the simulation.

The ice drift model (Eq. (10)) was used to incorporate the actual floe size and driving forces on April 5th, 2001. Visual

Table 2

Natural frequencies of the modes of the lighthouse model (Fig. 11) used in the simulations.

Mode	1,2	3,4	5,6	7,8	9,10	11,12	13,14	15,16	17,18	19,20	21,22	23,24
Frequency (Hz)	2.43	3.92	5.54	10.06	16.75	20.09	28.23	37.16	42.31	57.01	58.9	59.74

Table 3

Parameters used in the ice drift part of the model for simulation of the full-scale event of April 5, 2001 at the Norströmsgrund lighthouse.

$\rho_w(\text{kg m}^{-3})$	$C_{d,w}(-)$	$v_w(\text{m s}^{-1})$	$\rho_a(\text{kg m}^{-3})$	$C_{d,a}(-)$	$v_a(\text{m s}^{-1})$	$d_i(\text{m})$	$h_i(\text{m})$	$\dot{x}_{ice,0}(\text{m s}^{-1})$
1025	0.0025	0.4	1.29^3	0.002	7.5	780	0.9	0.1

observations defined a floe size of 800 m in drift direction and 500–600 m in transverse direction. Measurements indicate a floe thickness of 0.9 m. Coefficients for wind and air drag were defined based on [59] and the local current was estimated at 0.4 m s^{-1} . Ice model parameters shown in Table 1 (#5) were determined based on full-scale measurements of the STRICE campaign using the method outlined in Section 3.1. Parameters relevant for the ice drift model are defined in Table 3.

Simulation results for the global ice load and accelerations at the same two locations where the accelerometers were installed in 2001 are shown in Fig. 15, along with a close-up of the real measurements. The signals were filtered through a digital low-pass filter with a cut-off frequency of 150 Hz and resampled at 30 Hz corresponding to the technique applied for the full-scale measurements. As the ice floe slows down, as a consequence of the interaction with the structure, the initial continuous brittle crushing changes to frequency lock-in with the amplitude of the global force and acceleration of the structure increasing. The oscillation amplitudes simulated with the model are comparable to those measured in full-scale during lock-in. As soon as the ice floe comes to a stop, the global load reduces to zero in the model and the structural vibrations decay. In the model, a larger peak is observed before the ice floe comes to a rest which is not seen in the April 5th measurements, but this peak is not unphysical, as can be seen from measurements of the global load on an ice sheet slowing down against the Molikpaq structure [5]. To better capture the real interaction, the complete process needs to be accurately modelled, including larger failures and effect of pack driving forces. This is not possible with the presented model which only includes the effects of crushing in such detailed manner.

The analysis performed by Nord et al. [20] showed that, during the three years of the STRICE campaign, frequency lock-in developed 61 times, of which 98% of the cases at an ice drift speed between 0.02 and 0.06 m s^{-1} . To verify that the model can reproduce this general trend, we simulated the dynamic ice-structure interaction for ice drift speeds increasing from 0 m s^{-1} up to 0.15 m s^{-1} with 0.001 m s^{-2} predefined constant acceleration and with a mean brittle crushing load of 2, 4, and 6 MN, scaling the input parameters in Table 1 accordingly. This approach is chosen rather than simulating for constant drift speeds (Fig. 12b) as it gives a better indication of the critical drift speed for structures which are relatively stiff and heavy, and for which the limit cycle during frequency lock-in may not be reachable from the stable equilibrium of the structure. As most frequency lock-in events for the lighthouse were short in duration, we believe these were mainly due to favorable initial conditions. A similar range of critical drift

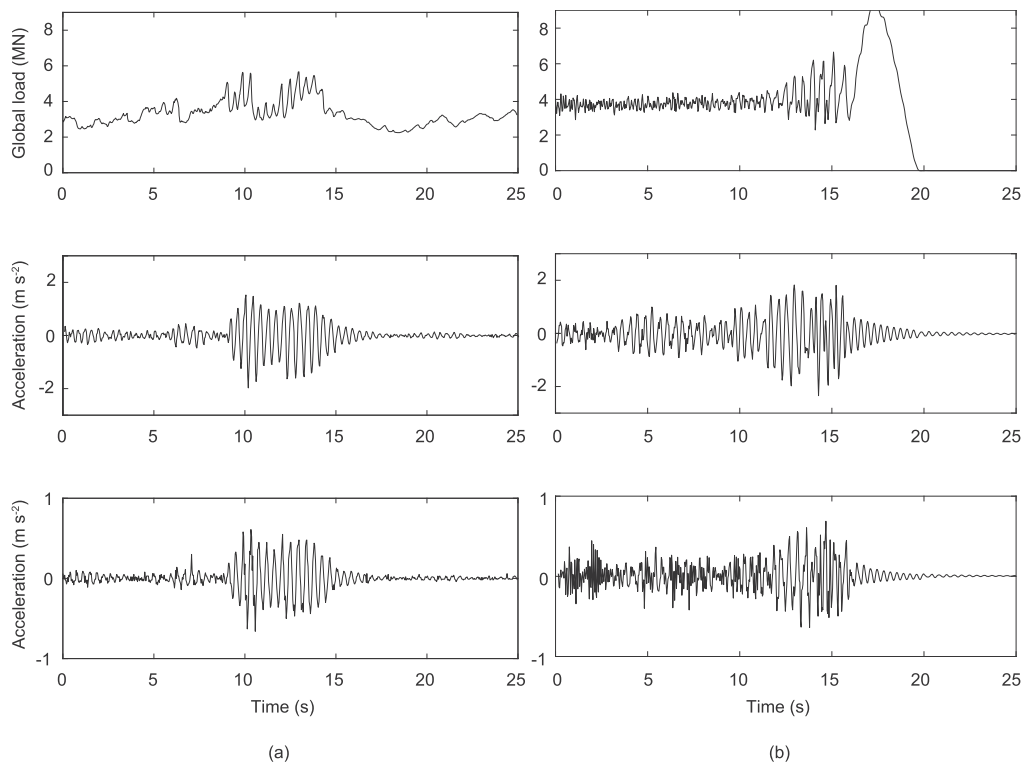


Fig. 15. An ice floe under the influence of environmental driving forces slowing down upon interaction with the Norströmsgrund lighthouse on April 5th, 2001. (a) Close-up of full-scale measurements in Fig. 13 and (b) simulation results.

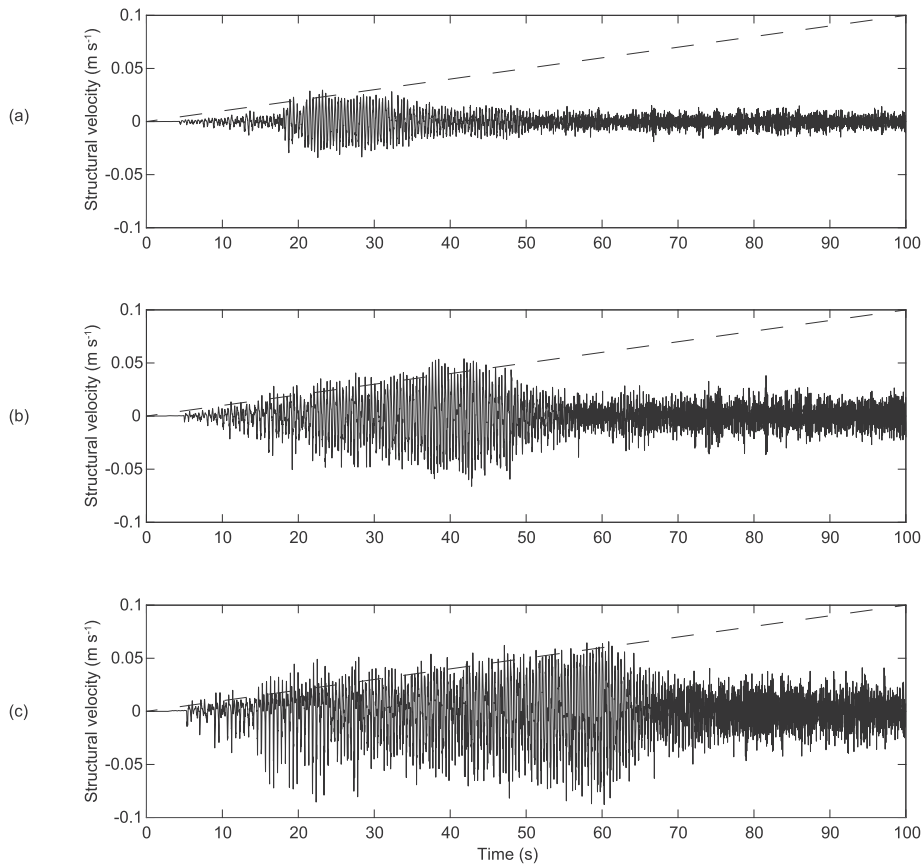


Fig. 16. Structural velocity in the direction of ice drift at the ice action point for simulations of constant accelerating ice sheets in interaction with the Norströmsgrund lighthouse at different levels of mean global ice load. The dashed line indicates the ice drift speed. The largest mean load results in the largest possible ice speed range for frequency lock-in as indicated in the plots. (a) 2 MN mean global load in continuous brittle crushing. (b) 4 MN mean global load in continuous brittle crushing. (c) 6 MN mean global load in continuous brittle crushing.

speeds for frequency lock-in to develop is obtained from the simulations as the one found from the full-scale data analysis (Fig. 16). For a load level of 2 MN, some amplification of the response is observed; however, the amplitudes only reach the level associated with sustained frequency lock-in for approximately 0.02 m s^{-1} ice drift speed. For 4 MN, frequency lock-in is obtained in the range of 0.02 m s^{-1} up to 0.045 m s^{-1} and for 6 MN the maximum drift speed is 0.06 m s^{-1} , approximately. Intermittent crushing is observed only for the highest load level of 6 MN in a very narrow range of drift speeds. There have been no reports of measured intermittent crushing during the full-scale campaigns.

6. Effect of floe size and environmental driving forces on ice-induced vibrations

Whilst in laboratory conditions, sustained ice-induced vibrations often develop, but for the Norströmsgrund lighthouse, the vibrations commonly lasted only for a small number of cycles [20]. Most of the pack ice interacting with the lighthouse came to a rest during interaction, as shown in Fig. 13. Other structures, such as the jacket platforms in the Bohai Bay [57], have shown to experience sustained frequency lock-in. The main difference between the two cases, besides the dynamic properties of the structures, is the magnitude of the ice load required to excite frequency lock-in. This load is relatively high for the Norströmsgrund lighthouse (Fig. 16) compared to the slenderer jacket structures. In order for sustained vibration to develop, the ice sheet or pack ice drifting towards the structure must remain both intact and keep its drift speed throughout the interaction. When the ice load on the structure is large, a larger load is acting on the ice, thereby slowing down the ice. Conditions for sustained vibration may then require significant driving forces or a large floe size.

Using the one-dimensional ice drift model (Eq. (10)), insights into the effect of floe size and driving forces on the development of ice-induced vibrations for the case of the Norströmsgrund lighthouse are obtained. The model considers only a single effective ice floe, representing either an individual ice floe or pack ice. In the latter case, the size of the equivalent floe can be taken equal to the pack size, accounting for ice concentration and only including those floes assumed to drift together. The model is a simplification of sea ice dynamics, being applicable when a limit stress situation develops in which the effective ice floe crushes against the structure. Rotation of floes, splitting, rafting, and internal stresses are not included in this approach, but are expected to limit the development

of ice-induced vibrations.

The most relevant scenario, from a design perspective, is that when sustained ice-induced vibrations develop. In such a scenario, the equilibrium drift speed of the ice floe needs to remain in the critical range where ice-induced vibrations develop for a given structure. In the case of the Norströmsgrund lighthouse, these critical ranges are shown in Fig. 16 for different levels of the mean brittle crushing load. The mean brittle crushing load is used here to reflect ice thickness and strength, where thicker and stronger ice results in a larger load. When the mean load during continuous brittle crushing μ_{cbr} is substituted for the ice load $F_{ice}(u_s, t)$ in Eq. (10), the equilibrium speed v_{eq} can be determined:

$$v_{eq} = \text{sgn} \left(\frac{\rho_a C_{d,a} v_a^2 - \frac{\mu_{cbr}}{\frac{\pi d_l^2}{4}}}{\rho_w C_{d,w}} \right) \sqrt{\left| \frac{\rho_a C_{d,a} v_a^2 - \frac{\mu_{cbr}}{\frac{\pi d_l^2}{4}}}{\rho_w C_{d,w}} \right|} + v_w \quad (13)$$

The equilibrium speed, determined this way, is an approximation as the mean global load during continuous brittle crushing is smaller than that during frequency lock-in and intermittent crushing. A negative or zero equilibrium speed indicates that the ice floe considered will come to a rest or stay at rest, depending on the initial conditions. This is the case for the Norströmsgrund example shown in Fig. 13, for which the equilibrium speed can be estimated based on Eq. (11), the parameters defined in Table 3, and the assumed mean global crushing load of 3.5 MN as $v_{eq} = -1.27 \text{ m s}^{-1}$. A positive equilibrium speed indicates that the ice floe will either accelerate or decelerate to that speed during interaction with the structure, depending on the initial conditions.

To illustrate the dependence of the equilibrium speed on effective floe size and driving forces, contour plots were made (Fig. 17). For making these plots, the values used in the Norströmsgrund simulations as defined in Table 3 were used in the drift model. Furthermore, a mean brittle crushing load of 4 and 6 MN were chosen, for which the critical range of ice speeds resulting in intermittent crushing and frequency lock-in were found to be between 0.02 and 0.045 m s^{-1} and 0.02 and 0.06 m s^{-1} as shown in Fig. 16b and c, respectively. Effective floe diameters of 780 m, 5600 m, and 11300 m were chosen: the first being equal to the floe size estimated for the example shown in Fig. 13, the second equivalent to a five by five square kilometer ice floe, and the third equivalent to a ten by ten square kilometer ice floe.

The contour plots show the relative importance of floe size over driving forces. For small floes, the currents need to be significant to generate enough driving force for an equilibrium condition to develop. For the floe of 780 m diameter, the current speed needs to be around 1.7 m s^{-1} to result in an equilibrium condition where sustained ice-induced vibrations may develop. Purely wind-driven ice would never result in a condition of sustained vibration for the range of wind speeds analyzed. For the scenario where the crushing load is 6 MN, all floes of size 780 m and smaller will come to a rest against the structure for the range of current and wind speeds considered. Considering the large floe sizes, it is found that the combinations of wind speed and current speed resulting in sustained ice-induced vibrations lie closer to the origin of the plots. This indicates that for larger floes, or pack ice in general, sustained vibration is much more likely to develop. Purely wind-driven ice only shows a very narrow range of wind speeds which may lead to sustained vibration, whereas for current-driven ice the range of speeds becomes significant and may easily lie within daily occurring ranges at a specific site.

For the Norströmsgrund lighthouse, the effective floe size required to generate sustained ice-induced vibrations at current speeds in the range of 0.4 m s^{-1} is in the order of five by five square kilometers. This is significant for the location of the lighthouse, providing an explanation why most incidents resulted in the ice coming to a rest and only a few cycles of frequency lock-in being observed. The effect of floe size on the development of vibrations is illustrated in Fig. 18 for the three points indicated in Fig. 17. The simulations were initiated with the floe drifting at 0.03 m s^{-1} towards the structure which is in the critical range for frequency lock-in developing. The small floe quickly comes to a rest, and the intermediate floe finds an equilibrium speed close to 0.03 m s^{-1} , causing significant vibrations. The large floe shows a number of cycles of vibrations after which the floe speed exceeds the critical speed for frequency lock-in and the structural response reduces.

7. Discussion

The presented example calculations illustrate that the developed model is applicable to a wide range of small-scale and full-scale scenarios. The model can be applied to simulate dynamic ice-structure interaction, provided that the phenomenological ice model parameters and the load level are defined correctly. This remains the main challenge, although we have developed approaches which show to give accurate results for model-scale and Baltic Sea conditions. The results presented, combined with our experience of applying the model to simulate ice-structure interaction, indicate that the input parameters may not vary significantly for different ice types, and that ‘scaling’ these parameters to account for the expected global ice load magnitude already gives good results. Research into dependencies of the model parameters on physical ice properties is, however, still ongoing, with the aim of better understanding these dependencies. It is research on local aspects of ice-structure interaction, such as area, roughness, friction, melting and recrystallization, which will hopefully allow to define relationships between physical ice properties and phenomenological model parameters as defined in Fig. 6 in the future.

To apply the model for simulations in the design of offshore structures, it is important to take into consideration the relevant design standards. Design load levels can be estimated based on [1] and incorporated in the model by adjusting the input parameters accordingly. This completely removes the uncertainty with respect to the load level, in which case the model is able to predict the interaction accurately. For conservative simulations of intermittent crushing and frequency lock-in with the model, three parameters can be adjusted. The transition speed of the ice can be increased in the model, leading to more severe vibrations at higher indentation

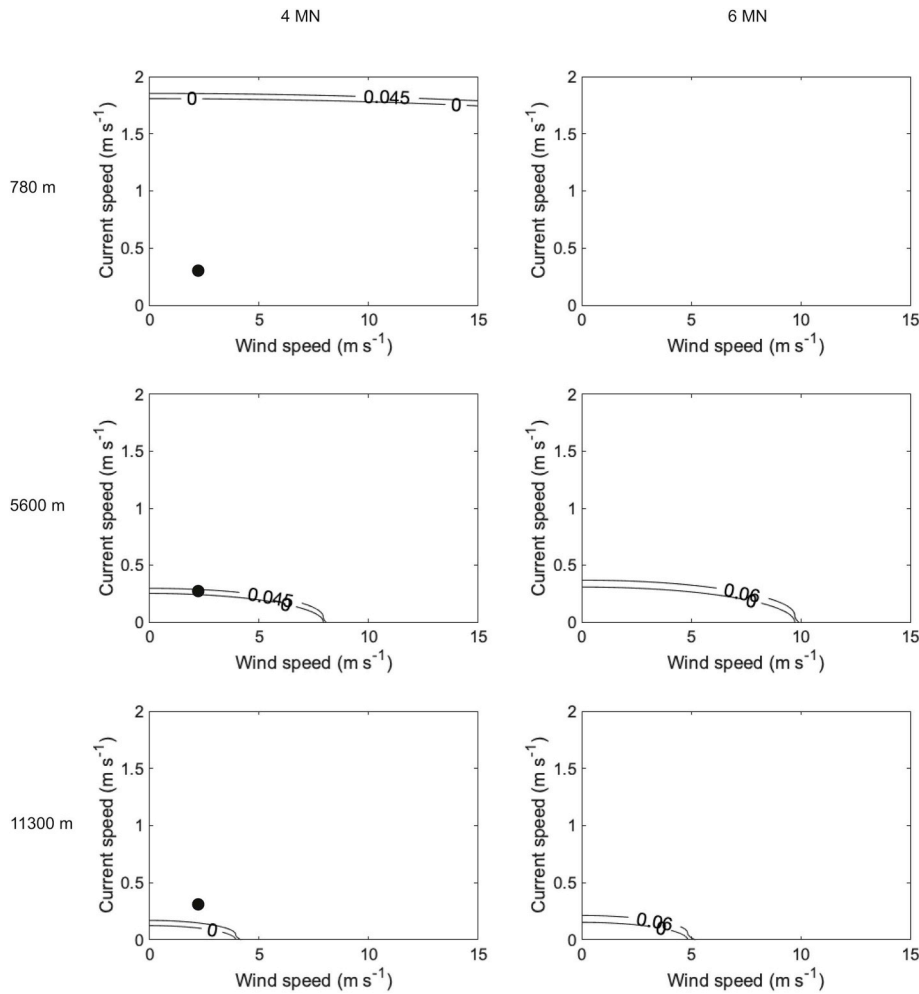


Fig. 17. Contour plots indicating combinations of wind speed and current speed resulting in equilibrium drift speeds required for sustained ice-induced vibrations. Left column: Assuming a 4 MN mean continuous brittle crushing load at high drift speeds. Right column: Assuming a 6 MN mean continuous brittle crushing load at high drift speeds. Three different floe diameters are shown. The lines bound the region of equilibrium drift speeds resulting in sustained ice-induced vibrations based on the analysis in Fig. 16. The black dots indicate the simulations presented in Fig. 18.

speeds. The ratio between the peak load and mean load can be increased in magnitude; however, we recommend a maximum of a factor four based on the in literature reported ratios between the contact area at high speed, and the maximum contact area at low speeds. Also, the slope of the mean global load in crushing can be reduced such that higher loads develop at higher ice drift speeds. For the critical deformation parameter, a low value results in more severe vibrations; however, this value is better defined taking into consideration the in full-scale measured frequency content of the ice load during continuous brittle crushing.

The presented model is limited to ice crushing, or pulverization, and does not explicitly incorporate larger failure mechanisms such as spalling, radial cracking, rubble pile up, and circumferential cracking. The option to include ice buckling has been explored in the past [15]; however, so far it has proven difficult to validate a model for combined buckling and crushing. We did not observe pure spalling in the model tests performed over the years, which may have resulted from the use of model ice. Nevertheless, we have observed plenty of frequency lock-in and intermittent crushing, indicating that the interaction is more governed by the pulverization of small-grained ice directly in contact with the structure rather than the larger failure events. For full-scale applications, it is of interest to expand the model to include the alternative failure modes as these result in larger reductions of the contact area and an increase in the standard deviation of the global ice load during continuous brittle crushing. The latter can only be captured with the current model by artificially increasing the value for the failure length, or reducing the number of ice elements.

Incorporation of the ice drift model allows for more realistic simulation of ice-structure interaction. The contour analysis presented shows that only few conditions may exist for which sustained vibrations can develop. Such analysis can have its impact in the design of offshore structures. Incorporation of ice drift this way can result in a significant reduction of estimates for fatigue damage by ice-induced vibrations when compared to assuming a constant ice drift speed. This is especially relevant for the accumulation of fatigue damage of structures in subarctic conditions where the size of individual ice floes or pack ice extent is limited. The one-dimensional model implemented here has limitations when it comes to simulating sea ice dynamics. However, when a large enough

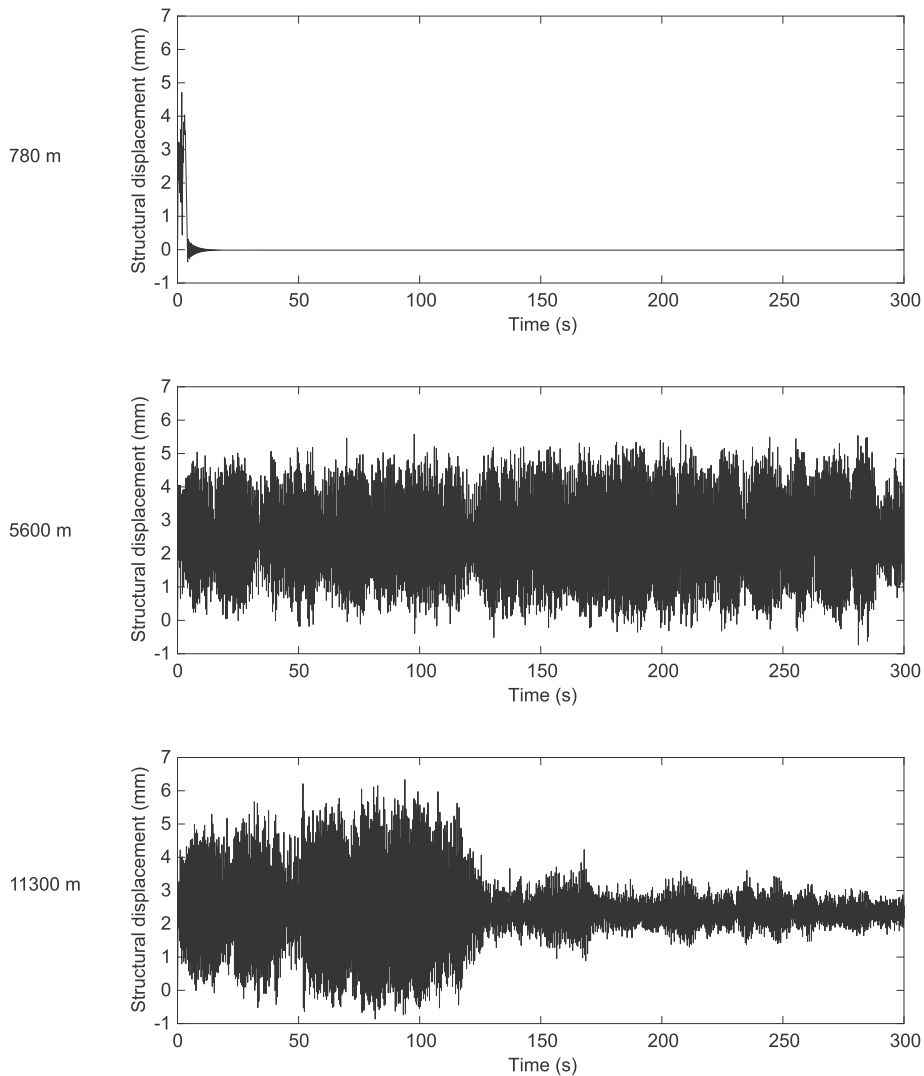


Fig. 18. Structural response at the waterline of the Norströmsgrund lighthouse for three different ice floe sizes and environmental conditions indicated in Fig. 17. The simulations are started with an initial floe speed of 0.03 m s^{-1} which is in the range of frequency lock-in.

size for the effective ice floe is considered, the model still provides a good estimate of the risks of sustained vibration developing since effects inside the ice pack such as rafting, splitting, and rotation are all limiting the driving forces, and hence the development of sustained ice-induced vibrations.

8. Conclusion

A model has been shown which can simulate the dynamic interaction between a drifting ice floe and a vertically sided offshore structure. Example calculations illustrate that the model captures all regimes of ice-induced vibrations. The model presented is based on experimental and full-scale observations showing that the contact between ice and structure depends on the speed of loading of the ice, in addition to the duration of loading at a specific speed. The presented model provides an alternative to existing models, and is unique in the sense that it does not contain parameters for defining the ice which depend on structural properties, thereby having a comparatively higher predictive value.

Simulation examples illustrate that the developed model captures the change from non-simultaneous to simultaneous failure associated with intermittent crushing, and the sawtooth pattern in load and displacement. The ice drift speeds for which frequency lock-in develops in model-scale and full-scale are predicted accurately, and the amplitude of oscillation follows the experimentally found frequency lock-in relation. The model captures the transition from continuous brittle crushing into frequency lock-in as observed when ice floes come to a stop during ice-structure interaction in full-scale scenarios.

The presented model can be used in the design of offshore structures, taking into consideration relevant design standards to determine the load level. It would be fruitful to perform additional research on the local interaction between ice and structures to

further improve on the description of local ice-structure interaction and reduce uncertainty with respect to the model input parameters. Additionally, the incorporation of larger failure events resulting in a significant change of the contact, such as spalling and circumferential cracking, as well as the natural variability in ice properties, will allow for an even more realistic simulation of full-scale ice-structure interaction.

Analysis of the effects of ice drift on ice-induced vibrations shows that floe size or pack ice extent has a significant influence on the development of sustained vibrations. This is specifically relevant for design and simulation of structures in subarctic conditions where pack ice extent, floe size, and driving forces are limited, in which case the inclusion of ice drift in the simulations may result in a significantly lower predicted fatigue damage when compared to assuming a constant ice drift speed.

Acknowledgements

This article presents the results of a combined fifteen years of work between its authors and we sincerely thank everyone who contributed over the years by kindly sharing their ideas, data, and critical notes to our work. In particular, we would like to thank the people involved from the start of SAMCoT in WP3 for their guidance: Andrei Metrikine, Mauri Määtänen, and Knut Høyland. We thank Cody Owen for his help in proofreading the article.

The authors wish to acknowledge the support of the Research Council of Norway through the Centre for Research-based Innovation, SAMCoT and the support of the SAMCoT partners.

The work described in this publication is also supported by the European Community's 7th Framework Programme through the grant to the budget of the Integrated Infrastructure Initiative HYDRALAB-IV, Contract no. 261520. The authors would like to thank the Hamburg Ship Model Basin (HSVA), especially the ice tank crew, for the hospitality, technical and scientific support, and the professional execution of the test programme in the Research infrastructure ARCTECLAB.

The full-scale measurements were funded by the European Commission DG RESEARCH under the Fifth Framework Program for Research and Development within the Energy, Environment and Sustainable Development (EESD) Program under the Key Action RTD activities of a generic nature (Contract No. EVG1-CT-2000-00024).

The authors wish to thank partners involved in the IVOS project: DNV GL, Engie SA, Kvaerner AS, Multiconsult AS, Shell Technology Norway AS, and Total E&P Norge AS.

Appendix A. Supplementary data

Supplementary data to this article can be found online at <https://doi.org/10.1016/j.marstruc.2019.01.012>.

References

- [1] ISO 19906. Petroleum and natural gas industries - arctic offshore structures. first ed. 2010. 2010-12-15.
- [2] IEC CDV 61400-3-1. Design requirements for offshore wind turbines. IEC document 88/642/CDV (Committee draft for vote of second edition of IEC 61400-3, now renumbered as IEC 61400-3-1). IEC TC88 WG03. first ed. 2017. 2017-07-28.
- [3] Matlock H, Dawkins WP, Panak JJ. A model for the prediction of ice-structure interaction. Proceedings of the first annual offshore Technology conference. 1969. p. 687–94. [Houston, Texas].
- [4] Gagnon RE. An explanation for the Molikpaq May 12, 1986 event. Cold Reg Sci Technol 2012;82:75–93.
- [5] techn Dr, Olsen Olav. Lessons-learned report for IIV JIP – phase 1. Technical report of the ice-induced vibrations JIP 2012. OO-11179-1.4.4. ,27 pages.
- [6] Jeong S, Baddour N. Comparison of characteristic failure frequency models for ice induced vibrations. JP J Solids Struct 2010;4(3):115–37.
- [7] Muhonen A. Evaluation of three ice-structure interaction models PhD thesis Helsinki University of Technology; 1996
- [8] Sodhi DS. An ice-structure interaction model. Mechanics of Geomaterial Interfaces 1995;42:57–75.
- [9] Määtänen M. Numerical model for ice-induced vibration load lock-in and synchronization. Proceedings of the 14th IAHR international symposium on ice, vol. 2. 1999. p. 923–30. [Potsdam, New York].
- [10] Kärnä T, Kamesaki K, Tsukuda H. A numerical model for dynamic ice-structure interaction. Comput Struct 1999;72:645–58.
- [11] Huang G, Liu P. A dynamic model for ice-induced vibration of structures. J Offshore Mech Arctic Eng 2009;131(1):6.
- [12] Withalm M, Hoffmann NP. Simulation of a full-scale ice-structure interaction by an extended Matlock-model. Cold Reg Sci Technol 2010;60:130–6.
- [13] Ji X, Oterkus E. A dynamic ice-structure interaction model for ice-induced vibrations by using van der pol equation. Ocean Eng 2016;128:147–52.
- [14] Hendrikse H, Metrikine A. Interpretation and prediction of ice induced vibrations based on contact area variation. Int J Solids Struct 2015;75–76:336–48.
- [15] Hendrikse H, Metrikine A. Ice-induced vibrations and ice buckling. Cold Reg Sci Technol 2016;131:129–41.
- [16] Hendrikse H, Ziemer G, Owen CC. Experimental validation of a model for prediction of dynamic ice-structure interaction. Cold Reg Sci Technol 2018;151:345–58.
- [17] Nord TS, Lourens E-M, Määtänen MP, Øiseth O, Høyland KV. Laboratory experiments to study ice-induced vibrations of scaled model structures during their interaction with level ice at different ice velocities. Cold Reg Sci Technol 2015;151:1–15.
- [18] Hendrikse H, Metrikine A. Edge indentation of ice with a displacement-controlled oscillating cylindrical structure. Cold Reg Sci Technol 2016;121:100–7.
- [19] Nord TS, Øiseth O, Lourens E-M. Ice force identification on the Norströmsgrund lighthouse. Comput Struct 2016;169:24–39.
- [20] Nord TS, Samardzija I, Hendrikse H, Bjerkås M, Høyland KV, Li H. Ice-induced vibrations of the Norströmsgrund lighthouse. Cold Reg Sci Technol 2018;155:237–51.
- [21] Løset S. Sustainable arctic marine and coastal Technology. Proceedings of the 24th international conference on port and ocean engineering under arctic conditions. 2017. POAC17-184, 14p.
- [22] Hendrikse H. Model for simulation of dynamic ice-structure interaction for vertically sided offshore structures – SDOF MATLAB implementation. Mendeley Data 2018. v1 <https://doi.org/10.17632/582m8565dj>.
- [23] Blanchet D, Churcher A, Fitzpatrick J, Badra-Blanchet P. An analysis of observed failure mechanisms for laboratory, first-year and multi-year ice. Proceedings of the IAHR ice symposium, vol. 3. 1988. p. 89–136. [Sapporo, Japan].
- [24] Timco GW. Laboratory observations of macroscopic failure modes in freshwater ice. Proceedings of the sixth international cold regions engineering specialty conference. 1991. p. 605–14. [West Lebanon, New York].
- [25] Schulson E, Duval P. Creep and fracture of ice. Cambridge university press; 2009.
- [26] Ponter ARS, Palmer AC, Goodman DJ, Ashby MF, Evans AG, Hutchinson JW. The force exerted by a moving ice sheet on an offshore structure part i. the creep

- mode. *Cold Reg Sci Technol* 1983;8:109–18.
- [27] Jordaan LJ. Mechanics of ice-structure interaction. *Eng Fract Mech* 2001;68:1923–60.
- [28] Sodhi DS. Crushing failure during ice-structure interaction. *Eng Fract Mech* 2001;68:1889–921.
- [29] Palmer AC, Goodman DJ, Ashby MF, Evans AG, Hutchinson JW, Ponter ARS. Fracture and its role in determining ice forces on offshore structures. *Ann Glaciol* 1983;4:216–21.
- [30] Kärnä T, Jochmann P, Kolari K. Observed ice – structure interactions in winters 2000 and 2001. Technical report, STRICE – devliberable No. D-3.1-A1_R-1-0. 2003. p. 69.
- [31] Timco GW. Indentation and penetration of edge-loaded freshwater ice sheets in the brittle range. *J Offshore Mech Arctic Eng* 1987;109(3):287–94.
- [32] Sodhi DS. Effective pressures measured during indentation tests in freshwater ice. Proceedings of the sixth international cold regions engineering specialty conference. 1991. p. 619–27. [Hanover, New Hampshire].
- [33] Gagnon RE. Consistent observations of ice crushing in laboratory tests and field experiments covering three orders of magnitude in scale. Proceedings of the 15th international conference on port and ocean engineering under arctic conditions, vol. 2. 1999. p. 12. [Helsinki, Finland].
- [34] Sodhi DS, Morris CE. Ice forces on rigid, vertical, cylindrical structures. Report 84-33, US army cold regions research and engineering laboratory. 1984.
- [35] Singh SK, Timco GW, Frederking RMW, Jordaan LJ. Tests of crushing on a flexible structure. Proceedings of the ninth offshore mechanics and arctic engineering symposium, vol. 4. 1990. p. 89–94. [Houston, Texas].
- [36] Takeuchi T, Sakai M, Akagawa S, Nakazawa N, Saeki H. On the factors influencing the scaling of ice forces. Proceedings of the IUTAM symposium on scaling laws in ice mechanics and ice dynamics, vols. 149–160. 2001. [Fairbanks, Alaska].
- [37] Sodhi DS, Takeuchi T, Nakazawa N, Akagawa S, Saeki H. Medium-scale indentation tests on sea ice at various speeds. *Cold Reg Sci Technol* 1998;28:161–82.
- [38] Blenkarn KA. Measurements and analysis of ice forces on Cook Inlet structures. Proceedings of the second annual offshore Technology conference, vol. II. 1970. p. 365–78. [Houston, Texas].
- [39] Finn DW, Jones SJ, Jordaan LJ. Vertical and inclined edge-indentation of freshwater ice sheets. *Cold Reg Sci Technol* 1993;22:1–18.
- [40] Izumiyama K, Uto S. Ice loading on a compliant indenter. Proceedings of the 16th international conference on offshore mechanics and arctic engineering, vol. 4. 1997. p. 431–6. [Yokohama, Japan].
- [41] Jefferies MG, Wright WH. Dynamic response of 'Molikpaq' to ice-structure interaction. Proceedings of the seventh international conference on offshore mechanics and arctic engineering, vol. 4. 1988. p. 201–20. [Houston, Texas].
- [42] Kamesaki K, Yamauchi Y, Kärnä T. Ice force as a function of structural compliance. Proceedings of the 13th IAHR International Symposium on Ice 1996;1:395–402. [Beijing, China].
- [43] Kärnä T, Muhonen A. Preliminary results from ice indentation tests using flexible and rigid indentors. Proceedings of the tenth IAHR international symposium on ice, vol. 3. 1990. p. 261–75. [Espoo, Finland].
- [44] Kärnä T, Kolari K, Jochmann P, Evers K-U, Xiangjun B, Määttänen M, Martonen P. Ice action on compliant structures. Research notes 2223, VTT technical research Centre of Finland. 2003.
- [45] Määttänen M. Modelling the interaction between ice and structures. Proceedings of the seventh international conference on port and ocean engineering under arctic conditions, vol. 2. 1983. p. 745–59. [Helsinki, Finland].
- [46] Muhonen A, Kärnä T, Eranti E, Riska K, Järvinen E, Lehmus E. Laboratory indentation tests with thick freshwater ice. Research Notes 1370, VTT Technical Research Centre of Finland. 1992.
- [47] Nakazawa N, Sodhi DS. Ice forces on flat, vertical indentors pushed through floating ice sheets. Special Report 90-14, US Army Cold Regions Research and Engineering Laboratory. 1990.
- [48] Toyama Y, Sensu T, Minami M, Yashima N. Model tests on ice-induced self-excited vibration of cylindrical structures. Proceedings of the seventh international conference on port and ocean engineering under arctic conditions, vol. 2. 1983. p. 834–44. [Helsinki, Finland].
- [49] Tsuchiya M, Kanie S, Ikejiri K, Yoshida A, Saeki H. An experimental study on ice-structure interaction. Proceedings of the seventeenth annual offshore Technology conference. 1985. p. 321–7. [Houston, Texas].
- [50] Yue Q, Bi X, Zhang X, Kärnä T. Dynamic ice forces caused by crushing failure. Proceedings of the 16th IAHR international symposium on ice, vol. 3. 2002. p. 231–7. [Dunedin, New Zealand].
- [51] Engellbrektson A. Observations of a resonance vibrating lighthouse structure in moving ice. Proceedings of the seventh international conference on port and ocean engineering under arctic conditions, vol. 2. 1983. p. 855–64. [Helsinki, Finland].
- [52] Huang Y, Shi Q, Song A. Model test study of the interaction between ice and a compliant vertical narrow structure. *Cold Reg Sci Technol* 2007;49:151–60.
- [53] Izumiyama K, Irani MB, Timco GW. Influence of compliance of structure on ice load. Proceedings of the 12th IAHR international symposium on ice, vol. 1. 1994. p. 229–38. [Trondheim, Norway].
- [54] Määttänen M, Järvinen E. Baltic aids-to-navigation ice-induced vibration measurements 2003. Report. Helsinki University of Technology; 2003.
- [55] Nordlund O-P, Kärnä T, Järvinen E. Measurements of ice-induced vibrations of channel markers. Proceedings of the ninth IAHR international symposium on ice, vol. 1. 1988. p. 537–48. [Sapporo, Japan].
- [56] Yue Q, Zhang X, Bi X, Shi Z. Measurements and analysis of ice induced steady state vibration. Proceedings of the 16th international conference on port and ocean engineering under arctic conditions. 2001. p. 413–21. [Ottawa, Canada].
- [57] Yue QJ, Li L. Ice problems in Bohai Sea oil exploitation. Proceedings of the 17th international conference on port and ocean engineering under arctic conditions. 2003. p. 13. [Trondheim, Norway].
- [58] Timco GW, Irani MB, Tseng J, Liu LK, Zheng CB. Model tests of dynamic ice loading on the Chinese JZ-20-2 jacket platform. *Can J Civ Eng* 1992;19:819–32.
- [59] Leppäranta M. The drift of sea ice. second ed. SPRINGER-PRAXIS BOOKS IN GEOPHYSICAL SCIENCES 978-3-642-04682-7; 2011. p. 370.
- [60] Määttänen M, Løset S, Metrikine A, Evers K-U, Hendrikse H, Løngøy C, Metrikin I, Nord T, Sukhorukov S. Novel ice induced vibration testing in a large-scale facility. Deciphering ice induced vibrations, part 1. Proceedings of the 21st IAHR International Symposium on Ice. 2012. p. 946–58. [Dalian, China].
- [61] Ziemer G. Research project IVOS – ice-induced vibrations of offshore structures 2017. p. 4. Technical Report <https://doi.org/10.13140/RG.2.2.34529.40801>.
- [62] Kärnä T. Full-scale data analyses of frequency lock-in. Technical Report of the Ice-Induced Vibrations JIP 2011. p. 94. OO-11179-1.2.2.

Update

Marine Structures

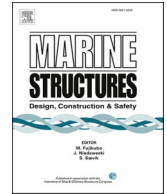
Volume 70, Issue , March 2020, Page

DOI: <https://doi.org/10.1016/j.marstruc.2019.102706>



Contents lists available at ScienceDirect

Marine Structures

journal homepage: <http://www.elsevier.com/locate/marstruc>

Corrigendum to “Dynamic response of an offshore structure interacting with an ice floe failing in crushing” [Mar. Struct. 65 (2019) 271–290]

Hayo Hendrikse^{a,b,*}, Torodd S. Nord^b

^a Department of Hydraulic Engineering, Delft University of Technology, Stevinweg 1, 2628, CN, Delft, the Netherlands

^b Sustainable Arctic Marine and Coastal Technology, Norwegian University of Science and Technology, Høgskoleringen 7A, 7491, Trondheim, Norway

The authors regret their mistake in the definition of the model parameters in Eq. (8) on page 277. The correct equation for the parameter C_2 is:

$$C_2 = \frac{F_t^3}{N^3 v_t}$$

The authors would like to apologise for any inconvenience caused.

DOI of original article: <https://doi.org/10.1016/j.marstruc.2019.01.012>.

* Corresponding author. Department of Hydraulic Engineering, Delft University of Technology, Stevinweg 1, 2628, CN, Delft, the Netherlands.
E-mail address: h.hendrikse@tudelft.nl (H. Hendrikse).

<https://doi.org/10.1016/j.marstruc.2019.102706>